Computational Materials Science 158 (2019) 289–295

Contents lists available at ScienceDirect

Computational Materials Science

journal homepage: www.elsevier.com/locate/commatsci

Phase-field simulation of non-isothermal phase separation in rapidly quenched Co-Cu melts

M. Krivilyov[a,b,*], D. Aflyatunova[c,a], V. Lebedev[a,b], P.K. Galenko[d]

[a] Udmurt State University, Department of Mathematics, Informatics and Physics, Universitetskaya str. 1, 426034 Izhevsk, Russia
[b] Udmurt Federal Research Center, Ural Branch, Russian Academy of Science, Baramzinoy str. 34, 426067 Izhevsk, Russia
[c] The University of Sheffield, Department of Automatic Control and Systems Engineering, Mappin street, Sheffield, UK
[d] Friedrich-Schiller-Universität Jena, Physikalisch-Astronomische Fakultät, D-07737 Jena, Germany

ARTICLE INFO

Keywords:
Phase separation
Undercooled melts
Rapid quenching
Phase-field model

ABSTRACT

Analysis of phase separation under non-isothermal conditions in undercooled molten Co-Cu droplets has been performed theoretically. The calculated microstructure length scales agree with the Cahn-Hilliard (CH) and Langer-Bar-on-Miller (LBM) models, and experimental data. At moderate cooling rates $V_c \sim 10^2 - 10^3$ K/s, the wave length $\lambda_m(t)$ of the fastest growing mode increases in time ($\partial\lambda_m/\partial t > 0$) in exact correspondence with the *isothermal* LBM model. At high K/s, λ_m slowly changes in time ($\partial\lambda_m/\partial t \sim 0$) in agreement with the *non-isothermal* CH model. At very high $V_c \sim 10^5 - 10^8$ K/s, initial decrease of λ_m ($\partial\lambda_m/\partial t < 0$) is first predicted. Then λ_m achieves its maximum value in time ($\partial\lambda_m/\partial t = 0$) and starts to increase ($\partial\lambda_m/\partial t > 0$) at the later stage. The revealed effect is examined and theoretically explained.

1. Introduction

Precipitation of the second phase from a uniform solid solution is known starting from the original studies by Hillert [1], Cahn [2], Skripov [3], Khachaturjan [4] and then by Ustinovshikov [5] and Binder [6]. As emphasized by Hillert in [7], a discovery of modulated microstructure became a new and partially unexpected result in an attempt to receive a robust thermodynamical description of interphase boundaries. The success in studying of this phenomenon known as spinodal decomposition is partially due to possibility of direct experimental observations. It was shown that the intensity I of X-ray scattering is proportional to the amplitude of the structure factor [8]:

$$I \sim \hat{S}(k, t) = \int d\mathbf{r}\, S(\mathbf{r}, t)\exp(i\,\mathbf{k}\cdot\mathbf{r}), \tag{1a}$$

$$S(|\mathbf{r} - \mathbf{r_0}|, t) = < \delta c(\mathbf{r}, t)\delta c(\mathbf{r_0}, t) >_V , \tag{1b}$$

$$\delta c(\mathbf{r}, t) = c(\mathbf{r}, t) - c_0, \tag{1c}$$

where $\hat{S}(k, t)$ is the Fourier image of the two-point correlation function $S(|\mathbf{r} - \mathbf{r_0}|, t)$ of fluctuations $\delta c(\mathbf{r}, t)$ of concentration c, c_0 is the initial chemical composition, $\mathbf{k}$ is the wave vector, t is the time and the averaging $\langle ... \rangle$ is performed over volume V. In experiments [5,9,8,10], the homogeneous solid solution Φ decomposes via $\Phi \rightarrow \Phi_1 + \Phi_2$ in two phases with formation of the modular $\Phi_1 + \Phi_2$ microstructure. Slow decomposition controlled by solid-state diffusion with a typical diffusion coefficient D of the order of $10^{-12} - 10^{-11}$ m/s^2.

Different phenomenological models of phase separation of solid solutions were suggested in literature [1–6] with a simple dependence of the free energy on temperature and concentration. The Cahn-Hilliard (CH) model [2] predicts exponential growth of all infinitesimal fluctuations δc with the wave numbers $k < k_c$. The critical wave number k_c defines the stability limit where all fluctuations with $k_m = k_c/\sqrt{2}$ are selected as the fastest growing mode. More recent experiments [5,6] revealed that the dynamics of the structure factor is accompanied by a shift of its maximum $\max|I(k, t)|$ to smaller k with time, i.e. $\partial k_m/\partial t < 0$. Later on, Langer, Bar-on and Miller (LBM) suggested the extended model [11] of phase separation accounted for fluctuations of chemical composition. The non-isothermal separation was analyzed by Huston, Cahn and Hilliard (CH) [12] and recently by Miranville et al. [13].

Phase separation was also widely experimentally studied in solidification of undercooled metallic melts [14]. During the last decade a new effect in phase separation has been revealed [15] and later reconfirmed [16,17]. If the particle size is about few nanometers then it substantially changes both the stability of material in the miscibility gap and its phase diagram. As a result, the binodal line can be discontinuous and phase separation does not occur in the samples sized

* Corresponding author at: Udmurt State University, Department of Mathematics, Informatics and Physics, Universitetskaya str. 1, 426034 Izhevsk, Russia (M. Krivilyov).
E-mail address: mk@udsu.ru (M. Krivilyov).

https://doi.org/10.1016/j.commatsci.2018.11.010
Received 16 July 2018; Received in revised form 25 October 2018; Accepted 4 November 2018

between 1 and 10 nm unlike to the macroscopic ones. Recently [18] separation in $Co_{50}Cu_{50}$ melts was analyzed using different quenching techniques including electromagnetic levitation (EML), quenching on a Pb-solder-coated copper chill substrate and splat-quenching. This provided new data on the kinetics of phase separation in the liquid state especially at early stages due to extra high quenching rates of the order of 10^6 K/s. For proper theoretical description of rapid phase separation under such cooling rates, the hyperbolic model of spinodal decomposition was suggested [19,20]. The model accounts for temporal relaxation of the diffusion flux and predicts non-linear behavior of the amplification rate in consistency with experimental data.

During high-rate quenching, non-isothermal and transient effects may drastically influence on the process of spinodal decomposition. We assume that the transient temperature field in rapid quenching may substantially shifts the maximum of the structure factor. This effect is not predicted by the linear models [2,11] and is not accounted for by the hyperbolic model [19]. To this end, the aim of this paper is analysis of phase separation in undercooled metal melts under rapid quenching. Comparison between the isothermal and non-isothermal cases is performed and the effect of quenching rate on microstructure is revealed. The analysis of phase separation in melts is compared to the results on phase separation in solid solutions.

2. Microstructure analysis

The parameters of the conducted experiments [18] on phase separation of deeply undercooled Co-Cu melts are as follow. Specimens of $Co_{50}Cu_{50}$ were alloyed from high-purity Co (99.995%) and Cu (99.999%) by electric arc melting under an Ar atmosphere at 980 mbar. The samples of about 1 g and 6 mm in diameter were tested using the EML technique in the chamber with He at 900 mbar. After heating of the sample above the melting temperature gas cooling by He is performed with the cooling rate of about $V_c \sim 10 - 20$ K/s. The first group of samples was tested in this regime and undercoolings up to 120 K were achieved. The second group was only slightly undercooled to temperatures below the critical point and quenched by contacting them with a Pb-coated copper substrate. For the third group of tests with production of rapidly quenched samples a splat-cooling device [21] has been installed below the levitation-coil system inside the EML chamber. This splat-cooling device allows us to reach the quenching rate of the order of $10^6 - 10^7$ K/s.

Microstructure analysis was done using scanning (SEM) and transmission (TEM) electron microscopy with the energy-dispersive X-ray spectrometry (EDS) system for precise analysis of chemical composition. The result given in Fig. 1 show that in the first group of samples a typical modulated microstructure typical for phase separation is registered, Fig. 1(a) with the characteristic scale of about 20–50 μm. The second group also evidences phase separation at the microscopic level however its morphology is drastically different. In the Cu-rich phase small spherical Co-rich precipitations were detected, Fig. 1(b).

The third group of samples obtained by splat cooling yields the modulated microstructure with a typical for spinodal decomposition texture, Fig. 1(c). XRD confirms coexistence of two Cu and Co-rich phases, Fig. 1(d), with a quasi periodic change of the chemical composition along any selected direction. Differently from two previous groups the interface has a complex worm-like structure which proves that the early or middle stage of separation was fixed experimentally. In some parts of the cross section small Co-rich globular structures of between 0.1 and 0.2 μm are detected in the bulk of the Cu-rich phase. Such twisted structures were registered in different parts of the sample and they are nearly oval with a diameter of about 0.29 μm in cross-sections, Fig. 1(c). The periodicity defined as a mean distance between two neighboring structures is about 0.4 μm.

Analysis by SEM using an InLens detector (secondary electrons) provided more accurate microstructure characteristics, Fig. 1. The average distance between Co-rich phases is 0.144 μm and the diameter of Co-rich "worm" structure is about 0.087 μm. Independent verification of these values was accomplished by TEM. After interpretation of the TEM data an estimate of 0.100 μm is received for a diameter of the Co-rich phase. The average TEM measured distance between the structures is in the range between 0.120 an 0.170 μm. Thus, in Ref. [18] it was demonstrated that early stages of phase separation in the liquid state can be registered experimentally in rapid quenching of metallic melts. In the present paper the data of experimental study [18] are compared with the results of numeric simulation to reveal the mechanism of phase separation under *non-isothermal* conditions.

3. Model

The phase-field model of phase separation $L \rightarrow L_1 + L_2$ in the miscibility gap is based [18,22] on the expression for the Gibbs free energy change ΔG suggested by Cahn et al. [23]

$$\Delta G(c, \nabla c, T) = \int \Delta g_{tot}\, dV = \int \left(\frac{1}{2}\varepsilon_c^2 |\nabla c|^2 + \Delta g_{bulk}(c, T)\right) dV, \tag{2a}$$

$$\Delta g_{bulk}(c, T) = -\beta(T_c - T)(\Delta c)^2 + \gamma(\Delta c)^4 + \eta(\Delta c)^6, \tag{2b}$$

where c is the relative concentration of the second component equal to the atomic fraction of Cu, $\Delta c = c - c_c$ is the deviation from the critical concentration c_c, ε_c^2 is the gradient-term coefficient, T is temperature and T_c is the critical temperature. The critical concentration and temperature are defined as the (c, T) point in the phase diagram where phase separation is firstly expected during melt cooling. The immiscibility gap in the Co-Cu phase diagram [14] is located beneath the liquidus. Below the bell-shaped binodal line a transition to phase instability occurs following the $L + \alpha(Co) \rightarrow L_1 + L_2$ reaction. For the Co-Cu alloy, the critical temperature and concentration are $T_c = 1547$ K and $c_c = 52.7$ at.% correspondingly [14].

The first (gradient) term in the integrand of Eq. (2) defines the density of excessive free energy at the interface between two phases. It is proportional to the squared concentration gradient and inverse proportional to the interface width squared. The bulk density Δg_{bulk} was chosen as a potential from the Landau–Devonshire theory which allows analysis at larger deviations from the equilibrium state than the classical Gizburg–Landau potential [24] does. The potential in Eq. (2)(b) is written as a Taylor expansion in the vicinity of the critical point as a function of undercooling $\Delta T = T_c - T$ and Δc at $T < T_c$. The positive coefficients β, γ and η of expansion are taken from [18].

The non-isothermal phase-field model accounting for fluctuations in the concentration field c is given by

$$\frac{\partial c}{\partial t} = -\nabla\cdot(-M\nabla\Psi) + Q(t, \mathbf{r}), \tag{3a}$$

$$\Psi = -\nabla\cdot\varepsilon_c^2\nabla c + \frac{\partial g_{bulk}}{\partial c}, \tag{3b}$$

$$T(t) = T_c - V_c t, \tag{3c}$$

where M is the atomic mobility, Ψ is the chemical potential, V_c is the cooling rate. The temperature of the melt is time-dependent but is considered as uniform in the microscopic volume on the scale of phase separation. Spatial uniformity of temperature is justified by a substantial difference in the characteristic scales of mass and heat transport. Accounting for the typical for metal values of the diffusion coefficient and thermal conductivity of $D \sim 10^{-9}$ m^2/s and $a \sim 10^{-6}$ m^2/s, the lengths of concentration and temperature inhomogeneity are reasonably estimated as D/V and a/V where V is the solidification or other characteristic velocity. Therefore, a difference in three orders of magnitude exists between the characteristic lengths.

Temperature fluctuations serve as a trigger mechanism to launch phase separation initially. In the present work, concentration fluctuations were instead included into the model. The term $Q(t, \mathbf{r}) = Q_t(t)Q_{\mathbf{r}}(\mathbf{r})$ in Eq. (3) is responsible for fluctuations of the

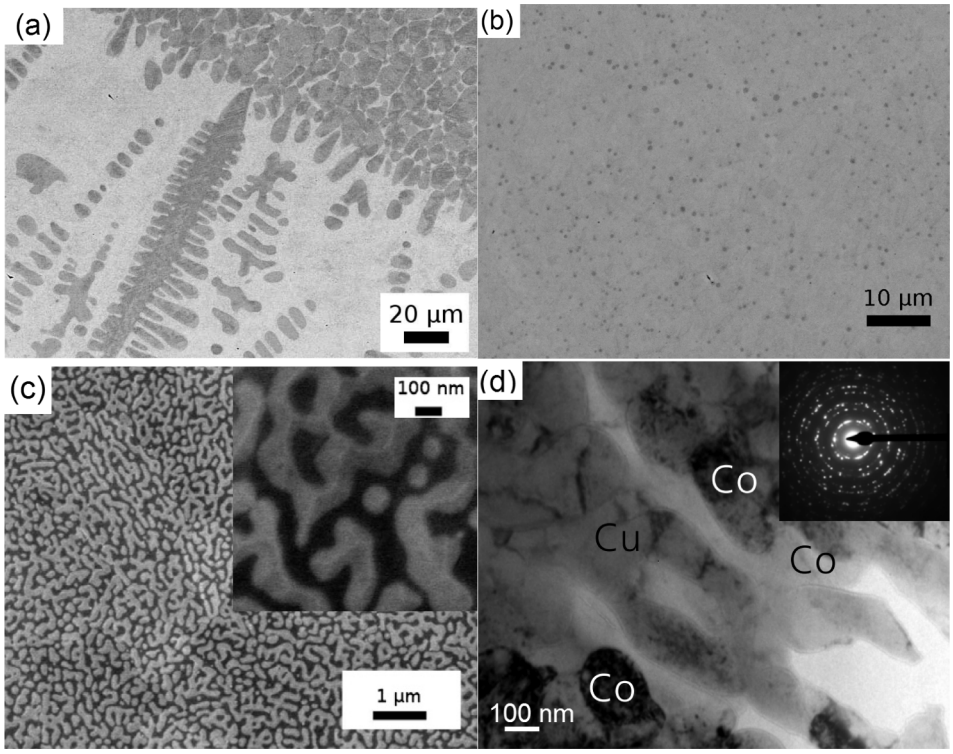

Fig. 1. Microstructure of the EML processed $Co_{50}Cu_{50}$ samples obtained by rapid quenching with different cooling rates V_c. Reprinted from [18], Copyright 2013, with permission from Elsevier. (a) Quenching from the undercooled state as a result of spontaneous or initiated solidification, $V_c \sim 10^1$ K/s. (b) Quenching through a contact with a copper plate, $V_c \sim 10^3 - 10^4$ K/s. (c, d) Quenching in a splat-cooling device, $V_c \sim 10^5 - 10^6$ K/s with Co-rich "worm" structure where (c) is SEM using an InLens detector (secondary electrons) and (d) Co and Cu-rich domains. The electron diffraction pattern in the inset corresponds to the Co-rich phase.

chemical composition. The time dependent term $Q_t(t)$ has a δ-function type and was activated every time when the temperature of the sample decreases by 1 K. The space dependent term $Q_{\mathbf{r}} = \xi_0 \xi(\mathbf{r})$ is defined using as a random variable $\xi(\mathbf{r}) \in [0, 1]$ and the fluctuation amplitude $\xi_0 \ll 1$. Thus at temperatures $T \geqslant T_c$ all fluctuations decays. Once the temperature decreases below T_c, the system becomes metastable and undergoes phase separation if a critical fluctuation develops.

All simulations were performed in 3D. The boundary-value problem is defined by uniform concentration $c = c_0$ and temperature $T = T_c$ at $t = 0$. The periodic boundary conditions yield continuity of the concentration and chemical potential at the opposite boundaries of the cubic computational domain. Laminar convective field is imposed assuming a weak linear profile typical for multiphase flow in confined geometries [25]. Therefore, the effect of convection on rapid phase separation is negligible and the convective term is omitted in Eq. (3).

Thermophysical parameters used in calculations of phase separation in Co–52.7 at.% Cu melt have been collected from literature and are as follows: the liquidus temperature $T_m = 1652$ K [26], critical temperature $T_c = 1547$ K [14], $c_0 = 52.7$ (at.%) [14], density $\rho = 7662$ (kg/m^3) [26], molar volume $V_m = 7.91 \times 10^{-6}$ (m^3/mol) [27,18], absolute viscosity $\mu = 0.0047$ (Pa·s) [28], kinematic viscosity $\nu = 6.1 \times 10^{-7}$ (m^2/s), surface tension [26,28], $\sigma = 1.3$ (N/m) [29], and diffusion coefficient $D = 10^{-8}$ (m^2/s) [30].

The model was solved in the direct space using the dimensional space coordinates and time measured in meters and seconds correspondingly. The dependent variables c and Ψ were scaled as c/c_c and Ψ/Ψ_0 where Ψ_0 is the estimated amplitude of the chemical potential. This transformation is necessary in order to avoid an ill-conditioned matrix in the numerical solution. The diffusion coefficient D and viscosity μ were used for calibrating of the phase field parameters. The constant mobility M is calculated using $D = -M/(\Delta g)''_{cc}$, where $(\Delta g)''_{cc}$ was found after thermodynamical assessment of the Co-Cu phase diagram.

As shown in literature [31], the linear correlation between generalized forces and fluxes accounting for the Gibbs-Duhem equation yields the nonlinear dependence of mobility on concentration $M(c) \sim c(1 - c)$. This effect is physically related to cross diffusion and often is complicated by thermo-diffusion [32]. In the concentration range around the initial concentration $c = c_c = 0.527$ at.% selected for present simulation, the mobility varies slowly and moreover its dependence is monotonic. It means that the dynamics of phase separation is slightly decelerated at the latest stage when selection of the fast-growing mode is already completed. Thus the results of simulations with the constant and concentration dependent mobilities should be similar. Other parameters of the phase-field model were chosen as follows: $\beta = 18$ J/(mol·K), $\gamma/\beta = 120$ K, $\eta/\beta = 1900$ K, $M = 0.58 \times 10^{-18}$ m^5/(J·s), $\varepsilon^2 = 10^{-8}$ J/m, $g_0 = 60$ J/mol, $L = 500 - 2000$ nm. Here L is the computational domain length. The model (3) was solved using the commercial software Comsol MultiPhysics [33] (licence No. 1056903).

The model was validated towards conservation of mass. The deviation of the mass balance was less than 0.001% with the eliminated fluctuation term. The numbers of degrees of freedom in simulations were 3×10^5 and 2×10^6 correspondingly within the domains 500 nm^3 and 2000 nm^3. The typical calculation time of all stages of phase separation was 24 and 600 h at the memory consumption of 4 and 40 Gb respectively. Postprocessing and evaluation of the correlation function were done in MATLAB with the specially developed code.

4. Results

In experiments on phase separation in solids the structure factor Eq. (1) is easily measured from low-angle X-ray scattering since the intensity I is proportional to the structure factor $\hat{S}(k, t)$. The intensity depends on the θ angle of scattering which is reduced to the wavenumber k using Wulff–Bragg's condition $k = (4\pi \sin\theta)/\lambda$, where λ is the

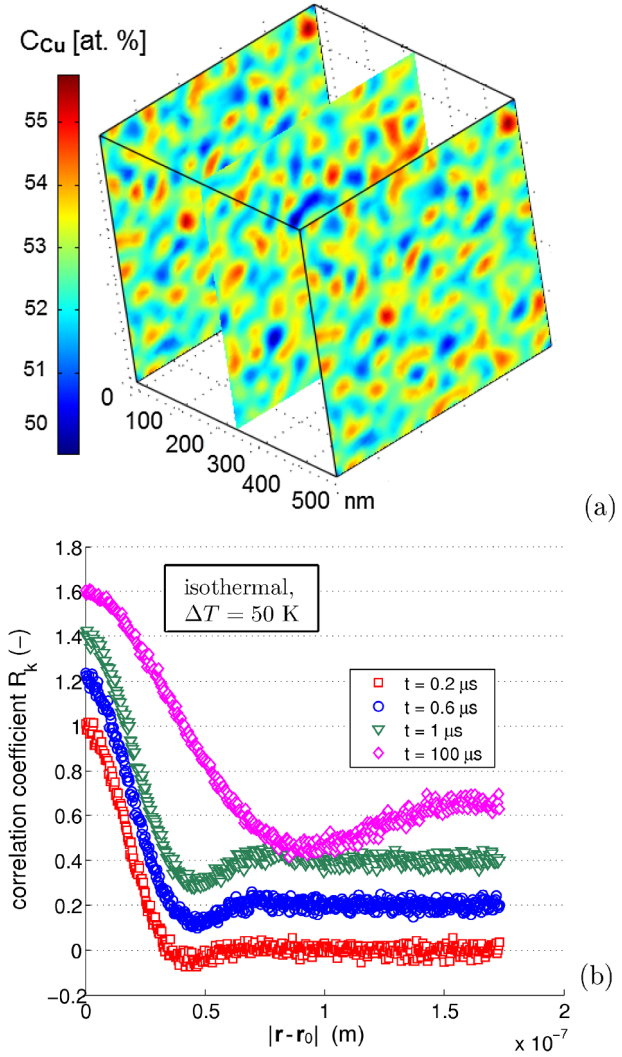

Fig. 2. Kinetics of phase separation calculated under *isothermal* conditions. The undercooling $\Delta T = 50$ K is constant. The domain size is $L^3 = 500^3$ nm^3. (a) Cross section of the concentration field at time of $t = 1$ μs. (b) Two-point correlation coefficient R_k given by Eq. (4) as a function of the distance $|\mathbf{r} - \mathbf{r_0}|$ between the points and is calculated at the different times *t.* of separation.

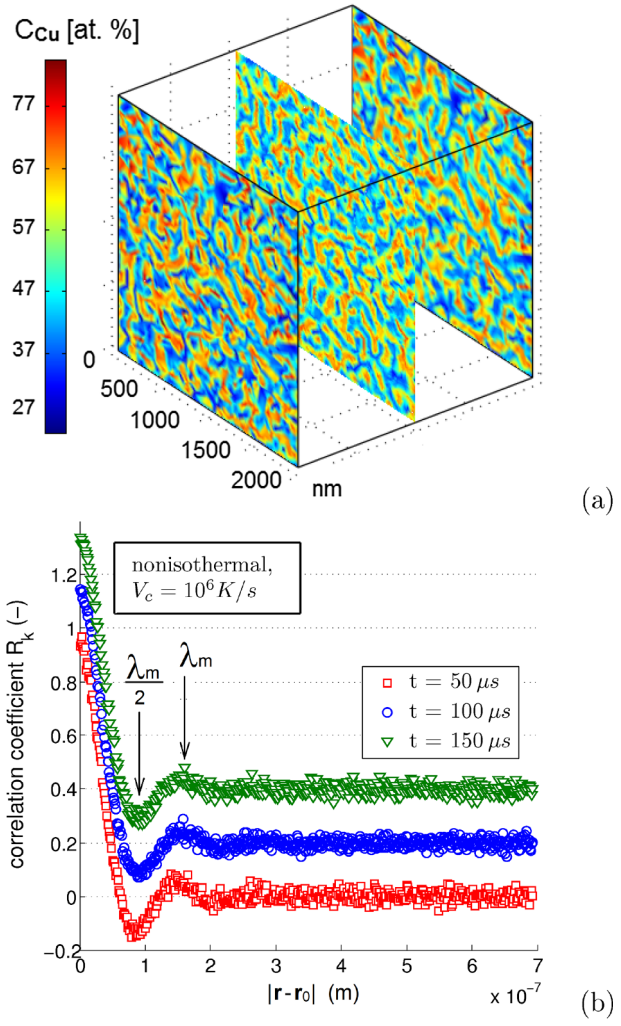

Fig. 3. Kinetics of phase separation calculated under *non-isothermal* conditions. The cooling rate is $V_c = 10^6$ K/s. The domain size $L^3 = 2000^3$ nm^3. (a) Cross section of the concentration field at time of $t = 50$ μs and an undercooling of $\Delta T = 50$ K. (b) Two-point correlation coefficient R_k given by Eq. (4) as a function of the distance $|\mathbf{r} - \mathbf{r_0}|$ between the points and is calculated at the different times *t.* of separation.

wavelength of X-ray radiation. Due to low speed of phase separation is solids, the kinetics of phase separation is easily tracked. In undercooled melts, phase separation in the liquid state is completed in few microsecond which does not allow *in situ* measurements of $\hat{S}(k, t)$. Hence, the behaviour of the structural factor can be reconstructed only via comparison of theoretical calculations with the microstructure of as-solidified samples.

In the present study, the diffusion Eq. (3) is solved in the direct (i.e. not Fourier) space. Thus, comparison between the CH, LBM and present models was done through the correlation length λ equal to the average distance between local concentration maxima. For this purpose, the two-point correlation function $S(|\mathbf{r} - \mathbf{r_0}|)$ defined by Eq. (1)b was first calculated. Then the correlation coefficient R_k depicted in Figs. 2 and 3 was found according to

$$
\begin{aligned}
&R_k(c(\mathbf{r})) = \frac{S(|\mathbf{r}-\mathbf{r_0}|)}{\sigma^2}, \quad k = 2\pi/|\mathbf{r} - \mathbf{r_0}|,\\
&S(|\mathbf{r} - \mathbf{r_0}|) = \frac{1}{V}\int (c(\mathbf{r}) - \bar{c})(c(\mathbf{r_0}) - \bar{c})\mathrm{d}V,\\
&\sigma^2 = \frac{1}{V}\int (c(\mathbf{r}) - \bar{c})\mathrm{d}\mathbf{r}, \quad \bar{c} = \frac{1}{V}\int c(\mathbf{r})\mathrm{d}\mathbf{r},
\end{aligned}
\tag{4}
$$

where k is the wave number. One can logically assume that the first minimum of $R_k(k)$ corresponds to one half $\lambda/2$ of the correlation length λ.

Fig. 2 shows the 3D distribution of c and $R_k(k)$ calculated for the same run at different times. Evolution of R_k is calculated at a constant undercooling $\Delta T = 50$ K in the domain of 500 nm^3 which corresponds to the scales observed experimentally in Fig. 1. The chosen time agrees to the characteristic time $\tau_{sep} = 0.98$ μs of phase separation [19] evaluated analytically. The correlation coefficient R_k has its first minimum at $|\mathbf{r} - \mathbf{r_0}| \sim 40$ nm with further increase to 100 nm at later times that matches well to the characteristic scale λ_{EXP} in the range $\lambda_{\mathrm{EXP}}100 - 200$ nm observed in the micrograph. The first three solutions in Fig. 2(b) correspond to the physical times of $t = 0$, 0.6 and 1.0 μs. In this time range, the location of the minimum of R_k varies slightly because the fastest growing mode was already selected and the phase separation proceeds actively. The last solution at $t = 100$ μs corresponds to the next stage of separation when microstructure coarsening as a result of minimization of the surface energy proceeds in the system.

For the validation of the present model, a comparison with CH and LBM models was first done under isothermal conditions at different undercoolings ΔT in the range from 1 to 150 K. A summary of the lengths λ_m calculated with the different models is provided in Fig. 4. Quantitatively, it is seen that the increase of ΔT up to 150 K leads to the drastic reduction of λ_m for all models. The present model, CH and LBM

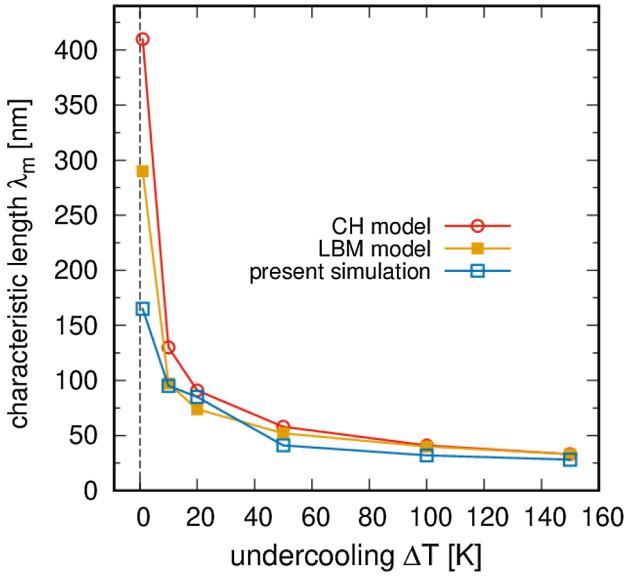

Fig. 4. Comparison of the characteristic microstructure scale λ_m of microsegregation calculated at *isothermal* conditions using the Cahn-Hilliard, Langer-Bar-on-Miller and present models. The value of ΔT gives an undercooling below the critical temperature and at the critical concentration. The comparison is performed at time of $t = 10^{-4}$ s for $\Delta T = 1,\ 10,\ 20$ K and $t = 10^{-6}$ s for $\Delta T = 50,\ 100,\ 150$ K.

models exhibit an essential difference only in the vicinity of the critical temperature, $\Delta T = 1$ K. It occurs due to the fact that these three models have a different contributions into spinodal decomposition close to the critical concentration and critical temperature. With the increase of ΔT, the critical wavelength λ_m given the maximum amplification rate is comparable for all three models. This shows that the selected length of spinodal structures is driven only by a deviation ΔT from the critical point for the investigated models.

Non-isothermal analysis was done under an assumption that fluctuations of temperature have a larger wavelength comparing to the wavelength of chemical composition in the selected computational domain. Thus the temperature in the domain is a function of time and spatially uniform, Eq. (3c)(c), and it was calculated with different cooling rates V_c estimated from the experiments shown in Fig. 1.

Fig. 3 yields the calculated kinetics of phase separation at a cooling rate of $V_c = 10^6$ K/s. The size of the computational domain is $2\,\mu m^3$ which is one order of magnitude larger than the correlation length of concentration inhomogeneity. Thus there are 10–15 modulations along the edge of the computational domain and the domain was representative. At the moment of $t = 50$ μs the undercooling is equal to 50 K. The correlation function at different times in Fig. 3(b) has the first minima at a constant value of $|\mathbf{r} - \mathbf{r_0}| = 90$ nm. The concentrational profiles analyzed at different times shows that the difference $(\max(c(\mathrm{r})) - \min(\mathrm{c}))$ increases with time. It happens due to a shift of the binodal concentrations of the L_1 and L_2 phases while the temperature of melt decreases. Therefore, this behaviour is in agreement with the non-isothermal CH model, where a constant wavelength is predicted at the beginning of separation with high cooling rates [12].

The analysis of phase separation under non-isothermal conditions of rapid quenching was performed at different cooling rates, Fig. 5. In this case the undercooling is an alternating function $\Delta T(t)$ of time t. At $V_c = 10^2$ K/s, the first minimum of the two-point correlation function $S(|\mathbf{r} - \mathbf{r_0}|, t)$ shifts to the right, the wave number k_m of the fastest mode decreases as the undercooling of the sample increases and this behaviour agrees with the LBM model. Additionally, for all depicted curves at $V_c \geqslant 10^5$ K/s the wave number first increases with time ($\partial k_m/\partial t > 0$). Next, k_m (or λ_m) achieves its maximum or minimum correspondingly, $\partial k_m/\partial t = \partial \lambda_m/\partial t = 0$, at selected undercoolings $\Delta T = \Delta T_x^*$, and then the kinetics changes as such that the modulation length grows ($\partial \lambda_m/\partial t > 0$, $\partial k_m/\partial t < 0$). This effect is registered in all calculations with high cooling rates $V_c \geqslant 10^5$ K/s and is not an artefact from particular simulations. Therefore, at $V_c \geqslant 10^5$ K/s an unusual kinetics of separation has been revealed, which by the author's knowledge was not reported earlier.

5. Discussion

The physical interpretation of the predicted effect is due to a change of the balance of atomic fluxes of the components controlled by the surface energy and back diffusion. Back diffusion is a process of atomic diffusion which results in the growth of concentration fluctuations. In the model, this effect is described by the first right-hand-side term in Eq. (3b)b where the minus sign represents the *back*, i.e. reversed to normal diffusion, direction of the process.

At the beginning of cooling, $\Delta T(t)$ is small thus the microstructure with a large λ_m is selected by the system because this is thermodynamically preferable. The large λ_m corresponds to the low or moderate concentration gradient $|\nabla c|$ is moderate. Therefore, the contribution of the gradient term in ΔG is limited. Under further cooling, the undercooling $\Delta T(t)$ of phase separation $L \rightarrow L_1 + L_2$ increases and the relative contribution of the gradient term in ΔG decreases. Thus, this facilitates the formation of finely modulated microstructure with small λ_m which becomes now favourable in terms of the total free energy ΔG. At the intermediate stages, back diffusion promotes microstructure coarsening and growth of λ_m and this process is opposite to microstructure refinement. Thus, a balance of these diffusion processes defines selection of the transient characteristic scale $\lambda_m(t)$ in time.

Under the isothermal conditions, the whole process of phase separation is accompanied by growth of $\lambda_m(t)$ in time. Under the non-isothermal conditions, $\lambda_m(t)$ first decreases and then starts to increase. The characteristic time for completion of spinodal decomposition [19] was estimates by us as $\tau_{sep} \sim 10^{-6}$ c. Since at cooling rates $V_c \geqslant 10^3$ K/s phase separation occurs rapidly, it was difficult to measure experimentally early stages of decomposition. Only quenching at $V_c > V_c^*$ where $V_c^* = \Delta T/\tau_{sep} \sim 10^6$ K/s allows to register the transients. Such experiments with the $Co_{50}Cu_{50}$ alloy quenched at variable $V_c = 10^1 ... 10^6$ K/s were reported in [18], see Section 2. For comparison with the experiment, simulations were done in the domains of 500 and 2000 nm^3. The nominal composition of the alloy in calculations was $Co_{48}Cu_{52}$ that corresponds to the critical composition for spinodal decomposition [18]. Since under splat cooling V_c is not measured directly, it was estimated as $V_c \sim 10^6$ K/s through back-of-the-envelope calculations [18].

Comparison of the present model with the LBM model and experimental data is given in Table 1, in which an average distance d_1 between the probes with maximum Cu concentration and the second distance d_2 as the average length of the Cu-rich phase are shown. In the present simulations, the microstructure length was chosen as a doubled length of the first minimum of the autocorrelation coefficient, see Fig. 2. In LBM, the length of microstructure was characterized by the wavenumber k_m. According to Table 1, the good agreement of the model simulations with experimental data is received at $V_c = 10^5 - 10^6$ K/s. Thus the present simulations have independently confirmed the estimated cooling rate of $V_c \geqslant 10^5$ K/s in splat quenching experiments [18] that supports accuracy of the developed phase-field formalism.

6. Conclusions

Theoretical study of non-isothermal phase separation in Co-Cu melt near the critical composition has been carried out under conditions of rapid quenching. Microstructure analysis of the splats (processed in EML and by splat quenching) evidences that the different stages of phase separation are observed experimentally. To show this, the effect

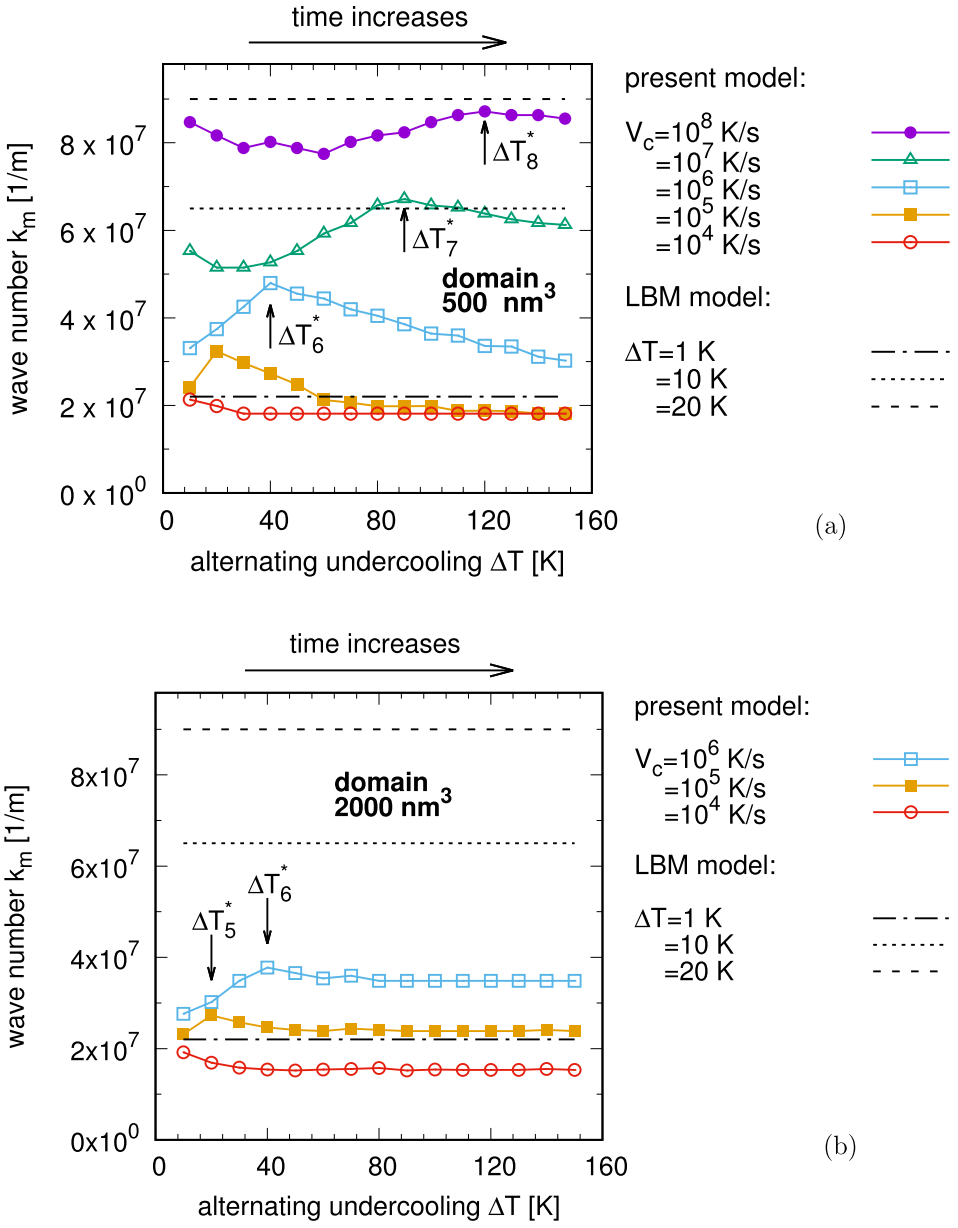

Fig. 5. Wave number k_m of the fastest growing mode as a function of the alternating undercooling ΔT of the sample and cooling rate V_c. In this plot, ΔT is a linear function $t = \Delta T/V_c$ of time t. ΔT_x^* with x equal to the power of V_c represent the critical undercoolings where the time-derivative $\partial k_m/\partial t$ changes its sign. Comparison with the *isothermal* LBM model at constant undercoolings of 1, 10 and 20 K is also provided. Analysis is performed in two calculation domains with a volume of (a) 500 nm^3 and (b) 2000 nm^3.

Table 1
Comparison of prediction λ_{LBM} and λ_{SIM} of the LBM and present models correspondingly performed at different cooling rates V_c to the characteristic microstructure scale λ_{EXP} registered experimentally [18]. The distance d_1 is the mean distance between neighboring spinodally decomposed patterns. The distance d_2 is the width of Co-rich bands.

LBM	Present simulation		Experiment
λ_{LBM}, nm	V_c, K/s	λ_{SIM}, nm	λ_{EXP}, nm
33 ÷ 52	10^6	82–93	SEM, InLens detector
	10^5	190–210	d_1 = 140, d_2 = 87
	10^4	210–210	bright-field TEM:
	10^2	450–450	d_1 = (120–170), d_2 = 100

of high cooling rates $V_c \geqslant 10^2$ K/s on the kinetics of phase separation in the liquid state was studied computationally.

Results of the developed phase-field model have showed the agreement with the classical CH and LBM models only within 30% and revealed a so-called "two-directional kinetics". Indeed, at cooling rates $V_c \geqslant 10^4$ K/s the wave length λ_m of microstructure qualitatively changes its dynamics during continuous cooling, and the revealed effect is explained by interplay of two different mechanisms of microstructure selection. First, cooling of the sample facilitates decrease of the length λ_m due to reduction of the interface contribution in the overall balance of the Gibbs free energy. Second, back diffusion in opposite facilitates the growth of λ_m. In case of small cooling rates $V_c \leqslant 10^2$ K/s or small undercoolings ΔT the second mechanism dominates thus the dynamic structure factor can be described by the isothermal LBM model. At high V_c the second mechanism is auxiliary since it is controlled by diffusion of the components with a finite speed of diffusion of the order of

$10^0 - 10^1$ m/s. The developed analysis is in agreement with the theory of continuously cooled liquids under phase separation [12] and extends it to deeply undercooled melts under rapid quenching.

Data availability

The raw/processed data required to reproduce these findings cannot be shared at this time due to technical or time limitations.

CRediT authorship contribution statement

M. Krivilyov: Conceptualization, Methodology, Software, Validation, Visualization, Writing - original draft. **D. Aflyatunova:** Formal analysis, Funding acquisition, Investigation, Methodology. **V. Lebedev:** Methodology. **P.K. Galenko:** Conceptualization, Supervision, Validation, Writing - review & editing.

Acknowledgments

This work was supported by the Russian Ministry of Science and High Education [Grant No. 11.6513.2017/BP], Russian Foundation of Basic Research [Grant Nos. 18-02-00643, 18-42-180002]; the Russian Space Agency and TSNIIMash [space experiment PERITECTICA (PARSEC)]; the Department of ACSE, Faculty of Engineering of the University of Sheffield; and the German Space Center Space Management [contract No. 50WM1541].

References

[1] M. Hillert, A solid-solution model for inhomogeneous systems, Acta Metall. 9 (1961) 525–535, https://doi.org/10.1016/0001-6160(61)90155-9.
[2] J. Cahn, Phase separation by spinodal decomposition in isotropic systems, J. Chem. Phys. 42 (1965) 93–99, https://doi.org/10.1063/1.1695731.
[3] V. Skripov, A. Skripov, Spinodal decomposition (phase transitions via unstable states), Usp. Fiz. Nauk 22 (6) (1979) 389–410, https://doi.org/10.1070/PU1979v022n06ABEH005571.
[4] A. Khachaturian, Theory of Structural Transformations in Solids, Wiley, 1974.
[5] Y. Ustinovshikov, S. Tresheva, Character of transformations in Fe-Co system, Mater. Sci. Eng. A 248 (1–2) (1998) 238–244, https://doi.org/10.1016/S0921-5093(98)00506-1.
[6] K. Binder, P. Fratzl, Phase Transformations in Materials, Weinheim, Wiley, 2001, https://doi.org/10.1002/352760264X.ch6 pp. 409–480 (Ch. Spinodal Decomposition).
[7] M. Hillert, A solid-solution model for inhomogeneous systems, Citation Classic 33 (1981) 18.
[8] M. Miller, J. Hyde, M. Hetherington, A. Cerezo, G. Smith, C. Elliott, Spinodal decomposition in Fe-Cr alloys: experimental study at the atomic level and comparison with computer models. I. Introduction and methodology, Acta Metall. Mater. 43 (9) (1995) 3385–3401, https://doi.org/10.1016/0956-7151(95)00040-3.
[9] T. Ujihara, K. Osamura, Kinetic analysis of spinodal decomposition process in Fe-Cr alloys by small angle neutron scattering, Acta Mater. 48 (2000) 1629–1637, https://doi.org/10.1016/S1359-6454(99)00441-3.
[10] O. Soriano-Vargas, E. Avila-Davila, V. Lopez-Hirata, H. Dorantes-Rosales, J. Gonzalez-Velazquez, Spinodal decomposition in an Fe–32 at.% Cr alloy during isothermal aging, Mater. Trans. 50 (7) (2009) 1753–1757.
[11] J. Langer, M. Bar-on, H. Miller, New computational method in the theory of spinodal decomposition, Phys. Rev. A 11 (4) (1975) 1417–1429, https://doi.org/10.1103/PhysRevA.11.1417.
[12] E. Huston, J. Cahn, J. Hilliard, Spinodal decomposition during continuous cooling, Acta Metall. 14 (1961) 1053–1062, https://doi.org/10.1016/0001-6160(66)90193-3.
[13] A. Miranville, G. Schimperna, Nonisothermal phase separation based on a microforce balance, Discrete Contin. Dyn. Syst. Ser. B 5 (3) (2005) 753–768, https://doi.org/10.3934/dcdsb.2005.5.753.
[14] C. Cao, G. Görler, D. Herlach, B. Wei, Liquid-liquid phase separation in undercooled Co-Cu alloys, Mat. Sci. Eng. A 325 (2002) 503–510, https://doi.org/10.1016/S0921-5093(01)01756-7.
[15] D. Burch, M. Bazant, Size-dependent spinodal and miscibility gaps for intercalation in nanoparticles, Nano Lett. 9 (11) (2009) 3795–3800, https://doi.org/10.1021/nl9019787.
[16] G. Radnoczi, E. Bokanyi, Z. Erdelyi, F. Misjak, Size dependent spinodal decomposition in cu-ag nanoparticles, Acta Mater. 123 (2017) 82–89, https://doi.org/10.1016/j.actamat.2016.10.036.
[17] E. Pogorelov, J. Kundin, M. Fleck, Analysis of the dependence of spinodal decomposition in nanoparticles on boundary reaction rate and free energy of mixing, Comput. Mater. Sci. 140 (2017) 105–112, https://doi.org/10.1016/j.commatsci.2017.08.028.
[18] E. Davidoff, P. Galenko, D. Herlach, M. Kolbe, N. Wanderka, Spinodally decomposed patterns in rapidly quenched Co-Cu melts, Acta Mater. 61 (4) (2013) 1078–1092, https://doi.org/10.1016/j.actamat.2012.10.010.
[19] P. Galenko, V. Lebedev, Non-equilibrium effects in spinodal decomposition of a binary system, Phys. Lett. A 372 (2008) 985–989, https://doi.org/10.1016/j.physleta.2007.08.070.
[20] N. Lecoq, H. Zapolsky, P. Galenko, Evolution of the structure factor in a hyperbolic model of spinodal decomposition, Eur. Phys. J. Special Top. 177 (2009) 165–175, https://doi.org/10.1140/epjst/e2009-01173-8.
[21] D. Herlach, H. Grill, G. Warmbold, B. Feuerbacher, German patent, no. 3723996, 1987.
[22] M. Krivilyov, E. Kharanzhevskii, V. Lebedev, D. Danilov, E. Danilova, P. Galenko, Synthesis of composite coatings using rapid laser sintering of metallic powder mixtures, Phys. Met. Metallogr. 114 (10) (2013) 799–820, https://doi.org/10.1134/S0031918X13080073.
[23] J. Cahn, Free energy of a nonuniform system. I. Interfacial Free Energy, J. Chem. Phys. 31 (1959) 688–699;
J. Cahn, Free energy of a nonuniform system. II. Thermodynamic Basis, J. Chem. Phys. 28 (1958) 258–267;
J. Cahn, Free energy of a nonuniform system. III. Nucleation in a Two-Component Incompressible Fluid, J. Chem. Phys. 30 (1959) 1121–1124, https://doi.org/10.1063/1.1744102.
[24] L. Landau, E. Lifschitz, Statistical Physics, Part 1, third ed., Pergamon Press, 1980.
[25] S. Lomaev, M. Krivilyov, J. Fransaer, Exact analytical solution based on the vector potential technique for a conjugated hydrodynamic and joule heating problem in an electromagnetically levitated drop, Magnetohydrodynamics 52 (1) (2016) 105–116, https://doi.org/10.22364/mhd.
[26] J. Brillo, I. Egry, T. Matsushita, Density and excess volumes of liquid copper, cobalt, iron and their binary and ternary alloys, Int. J. Mater. Res. 97 (2006) 11, https://doi.org/10.3139/146.101415.
[27] D. Lide, Handbook of Chemistry and Physics, CRC Press, 2008.
[28] M. Schlick, J. Brillo, I. Egry, Thermophysical properties of liquid Co-Cu-Ni alloys, Int. J. Cast Met. Res. 22 (2009) 82, https://doi.org/10.1179/136404609X367380.
[29] J. Brillo, I. Egry, Density and surface tension of electromagnetically levitated Cu-Co-Fe alloys, Int. J. Thermophys. 28 (3) (2007) 1004–1016, https://doi.org/10.1007/s10765-007-0209-8.
[30] M. Kolbe, C. Cao, P. Galenko, J. Fransaer, D. Herlach, Dynamics of solidification and microstructure evolution in undercooled Co-Cu alloys with metastable miscability gap, in: P.T. et al. (Eds.), Proc. of the EPD Congress 2002 and Fundamentals of Advanced Materials for Energy Conversion, Washington, 2002, pp. 539–553.
[31] L. Granasy, T. Pusztai, J. Warren, Modelling polycrystalline solidification using phase field theory, J. Phys.: Cond. Matt. 16 (41) (2004), https://doi.org/10.1088/0953-8984/16/41/R01.
[32] B. Smorodin, S. Ishutov, I. Cherepanov, B. Myznikova, Convection of a colloidal suspension in a hele-shaw cell, Eur. Phys. J. E Soft Matter 40 (18) (2017), https://doi.org/10.1140/epje/i2017-11502-0.
[33] Comsol Modelling Guide. Version 3.5a., Comsol Inc., 2008.